Forces in Mechanics 6 (2022) 100063

Contents lists available at ScienceDirect

Forces in Mechanics

journal homepage: www.sciencedirect.com/journal/forces-in-mechanics

In situ investigation of chemical composition during TIG welding in duplex stainless steels using Laser-Induced Breakdown Spectroscopy (LIBS)

Lukas Quackatz *, Axel Griesche, Thomas Kannengiesser

9.4 Weld Mechanics, Federal Institute for Materials Research and Testing, Unter den Eichen 87, Berlin 12205, Germany

ARTICLE INFO

Keywords:
LIBS
TIG welding
Duplex stainless steels
In situ measurement
WRC-1992-diagram

ABSTRACT

Many applications in industry require a material-to-material joining process of Duplex Stainless Steels (DSS). Therefore, it is essential to investigate the material's properties during a welding process to control the weld quality. With the help of Laser-Induced Breakdown Spectroscopy (LIBS), the chemical composition during the Tungsten Inert Gas (TIG) welding process of DSS could be monitored *in situ*. The chemical composition could be quantitatively measured using pre-established calibration curves. Although the surface temperature and the welding plasma have a high influence on the spectral intensities, reliable composition measurements were possible. The concentration of alloying elements could be mapped during the TIG welding process.

1. Introduction

Duplex stainless steels (DSS) have a balanced proportion of ferrite (α) and austenite (γ). This property realizes high strength combined with good corrosion resistance in a temperature range of −50 °C–1300 °C [1]. These properties make DSS superior to other corrosion resistant stainless steels. In the past decade has been a lot of research performed related to the further development and optimization of DSS. In addition to improving corrosion resistance, the aim was also to reduce costs and increase the economic efficiency of DSS. For these reasons, the material class of Lean Duplex was created. The Ni concentration is reduced, and Ni is substituted by Mn. Furthermore, the Mo concentration is reduced compared to standard duplex [1,2]. The subject of this research is both Standard Duplex (EN grade 1.4462) and Lean Duplex (EN grade 1.4162).

A large number of applications in industry require a welding process of the DSS. Due to the rapid cooling of the weld metal and the additional nitrogen effusion from the molten pool, the ferritization of the weld metal is too domaining. Due to the high N concentration and the low Mo concentration, the Lean Duplex exhibits improved austenite formation during solidification [3].

The properties and weldability of DSS depend particularly on the ferrite content of the material. For example, to avoid hot cracks, a minimum ferrite content must be present after welding. Furthermore, the ferrite content has an influence on the subsequent properties of the welded component in service. Microstructure development in high-temperature service, carbide precipitation and σ-phase formation are of high interest. If these problems are not considered, embrittlement of the material and premature failure of the component will occur. In addition, ferrite content affects corrosion resistance and low-temperature toughness. An imbalance in the α/γ-distribution can lead to a significant reduction in the local physical properties of DSS. Thus, even the slightest elemental burn-off during welding can cause critical changes in the chemical composition and phase ratio in DSS. Yang et al. [4] have shown that the non-uniform distribution of an α/γ-ratio with 80–90vol.% ferrite in the weld metal causes significant cracking problems in safety-related components. Martin et al. [5] have shown that the high temperature fracture strength of DSS increases dramatically with increasing γ-vol.%. Since the chemical properties, such as corrosion resistance and high strength values are the main reasons for preferring DSS, this α/γ ratio must be kept constant during and after welding in the Fusion Zone (FZ) and Heat Affected Zone (HAZ), respectively. By changing the chemical composition of the weld metal and the temperature control during welding, the ferrite content can be controlled [6–8].

The risks previously stated have raised the need to develop predictive tools for the ferrite content in the weld microstructure of steels. Currently, various constitution diagrams exist, such as the Schaeffler diagram [9], the De Long diagram [10] and the WRC-1992 diagram [11]. All diagrams are based on the calculation of chromium (Cr_{eq}) and nickel equivalents (Ni_{eq}). They differ in the calculation method of Cr_{eq} and Ni_{eq} from the chemical composition of the material. Table 1 shows the calculation methods for the different constitution diagrams.

Currently, the most used tool for predicting ferrite content after

* Corresponding author.
E-mail addresses: Lukas.quackatz@bam.de (L. Quackatz), axel.griesche@bam.de (A. Griesche), thomas.kannengiesser@bam.de (T. Kannengiesser).

https://doi.org/10.1016/j.finmec.2021.100063
Received 11 November 2021; Received in revised form 8 December 2021; Accepted 8 December 2021
Available online 17 December 2021

Table 1
Creq and Nieq formulae used for estimating ferrite content from constitution diagrams [12,13].

Constitution diagram	Cr_{eq} formula	Ni_{eq} formula
Schaeffler (1949)	$Cr_{eq} = Cr + Mo + 1.5Si + 0.5Nb$	$Ni_{eq} = Ni + 30C + 0.5Mn$
DeLong (1973)	$Cr_{eq} = Cr + Mo + 1.5Si + 0.5Nb$	$Ni_{eq} = Ni + 30C + 30\,N + 0.5Mn$
WRC-1992	$Cr_{eq} = Cr + Mo + 0.7Nb$	$Ni_{eq} = Ni + 35C + 20\,N + 0.25Cu$

welding of stainless steels is the WRC-1992 diagram [11]. Based on calculated Cr_{eq} and Ni_{eq}, a ferrite number (FN) is estimated.

The FN corresponds to the volume fraction of ferrite in the steel. It is standardized and determined using a defined measuring method. The FN is based on the magnetic attraction of the ferrite phase in the steel [14].

In recent years, researchers have shown that the Cr_{eq} and Ni_{eq} coefficients for the WRC-1992 diagram are not accurate and therefore need to be adjusted [15]. According to Kotecki and Siewert [11,16] two relevant areas need to be further developed:

1 The effect of the cooling rate is not considered in the WRC-1992 diagram. However, during solidification of the weld metal, the cooling rate has a great influence on the resulting microstructure. This has already been demonstrated by Balmforth and Lippold [17].
2 The inaccuracy of the WRC-1992 diagram in relation to other alloying elements, e.g., Si, W, Ti, which, however, have a significant impact on the final ferrite content of the weld metal.

Furthermore, the Cr_{eq} and Ni_{eq} coefficients are constant, i.e., the use of filler metals cannot be calculated. This method of predicting phase distributions is open to further development. Therefore, many studies are concerned with improving the prediction of weld microstructrue [18–20].

Since current analysis methods for welded components either predict the ferrite content too inaccurately or are based on postmortem examination methods, such as metallographic determination of the ferrite content [17,21,22], *in situ* measurement methods for the analysis of welded components are of high relevance. Furthermore, none of the prediction capabilities developed are spatially resolved and can visualize local enrichments. LIBS offers one possibility. It enables highly accurate, quasi-destructive, time- and spatially resolved quantitative measurements of the chemical composition during welding, i.e., before/during/after solidification of the weld metal in the FZ and HAZ.

LIBS is a spectroscopic method with which elemental compositions can be determined. A high-energy pulsed laser is used to create a microplasma on the surface of the material under investigation. As the plasma cools and decays over time, it begins to emit element-specific radiation. This radiation can be resolved and detected with a spectrometer [23]. The measurement method can be calibrated using certified reference materials so that quantitative measurements can be realized. In the context of Industry 4.0, the digitization of the welding process is essential. LIBS offers a possibility to perform *in situ* measurements during welding and to ensure error-free welding processes. Previous research by Taparli et al. [24,25] has shown that *in situ* LIBS measurements during TIG welding are possible. Differences of the different welding zones (weld metal, heat affected zone) could be shown in LIBS spectra. The intensities of the main alloying elements chromium, nickel and manganese could be shown with time resolution. Furthermore, the burn-off of alloying elements during the welding process could be revealed [26].

The intensities from the LIBS spectra depend on the surface temperature of the sample [27–29]. Therefore, the electron temperature in the plasma can be correlated with the surface temperature of the sample. This makes it possible to detect and record the surface temperature and the cooling curve using LIBS measurements. Recent studies are already using electron temperature as an analysis tool in welding technology [30–33]. For example, Lednev et al. [32,33] performed *in situ* LIBS measurements during laser welding of steel plates. They were able to distinguish defective from defect-free welds with the help of spectra evaluation. For this purpose, different iron lines were evaluated in a time-resolved manner and a clear difference between the defective and defect-free welds could be highlighted. Furthermore, the electron temperature in the plasma was used as an analysis method. This showed a clear difference between defective and defect-free welds. In addition, the different temperature cycles during the welding process could be identified in the electron temperature curve. For the optimization of the WRC-1992 diagram, both the chemical analysis by LIBS and the calculation of the electron temperature will be used.

Tungsten Inert Gas (TIG) welding is a conventional and preferred technology for welding DSS because it is economical and simple to implement in a manufacturing process. During the TIG process, an arc is formed between a non-melting tungsten electrode and the material to be welded and shielding gas (Ar or He) is supplied via a torch to protect the weld pool and electrode from oxidation. If a filler wire is used, it is fed separately to the weld pool. The most important process parameters are the welding current, the welding speed and the shielding gas flow rate [34].

Based on the previous research, further experiments are carried out with duplex steels and quantitative measurements are realized using certified reference materials (CRM). For this purpose, an experimental setup is used that allows *in situ* LIBS measurement during TIG welding.

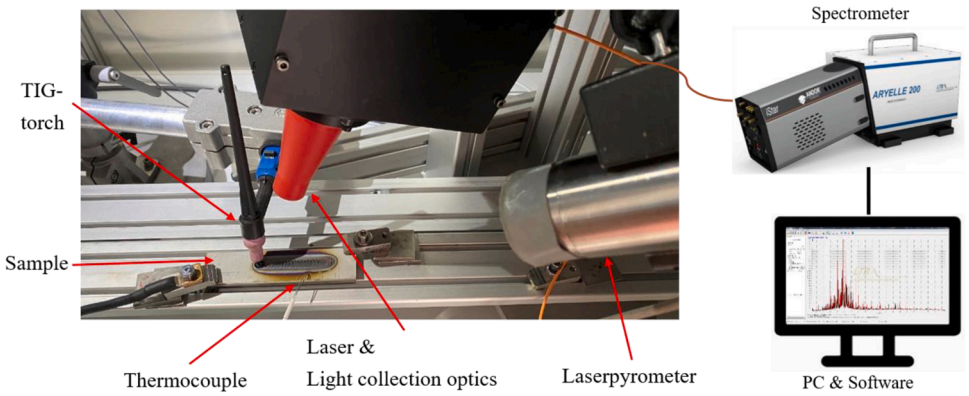

Fig. 1. Experimental setup for the *in situ* LIBS measurement during TIG welding.

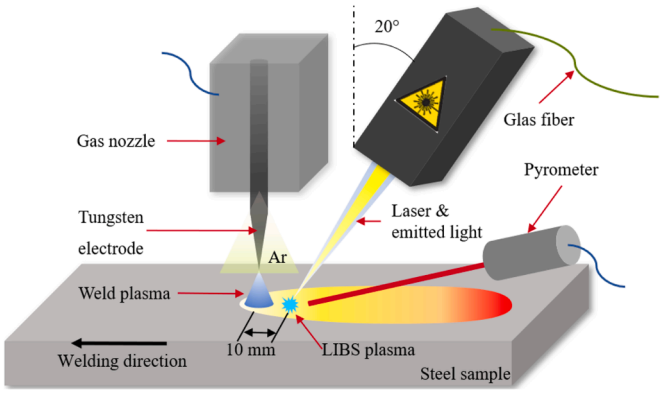

Fig. 2. Experimental sketch of the LIBS and weld setup.

2. Material and methods

2.1. Material

EN grade 1.4462 and 1.4162 duplex stainless steels were selected as sample material. Due to the outstanding physical properties of duplex steels, they are used in almost all branches of industry. Examples include power plant components, maritime structures and various welded structures. The chemical composition of the samples used can be seen in Table 2.

Flat specimens (length x width x thickness = 150 × 35 × 5 mm^3) were made from the material used. Immediately before welding, these were cleaned with acetone.

2.2. Experimental

The experimental setup of the *in situ* LIBS experiments is shown as a photo in Fig. 1. The LIBS setup consists of a pulsed Nd:YAG laser (1064 nm, 15 Hz) with an average power of 5 W. The maximum energy per pulse is 200 mJ. The laser used is from Quantel USA. A LIBS controller and an Aryelle 200 echelle spectrometer from LTB Berlin are connected. Due to the high detection accuracy and the low signal noise, an ICCD detector from Andor was used [35]. The laser beam was focused on the sample surface using an optical focusing and light collection system, with a focal length of 300 mm. Then focused on the fiber optic connector using the same system, with a focal length of 10 mm. Due to the additional electromagnetic radiation of the welding plasma, optical filters are built into the optics of the laser. This setup was connected to the spectrometer. Twenty laser shots were accumulated per measurement. The optimum settings for gate width and delay time could be determined from experiments carried out in advance. The gate width was 20 µs and the delay time 1 µs.

The welding experiments were performed with a Tungsten Inert Gas (TIG) welding system Castolin CastoTIG 1611 DC power supply with Castolin TIG torch using a pure tungsten electrode with 1.6 mm diameter. Fig. 2 shows the welding configuration. The distance between the base metal and the electrode tip was set to 5 mm. The electrode tip protruded about 3 mm from the ceramic gas nozzle (diameter 6 mm). All welding operations were performed with a constant Ar shielding gas flow of 10 l/min. The welding torch and laser are rigidly mounted. The laser is inclined at 20°, normal to the surface of the specimen. The specimen lay on a table that could be moved in a defined direction with the help of a linear motor.

DSS specimens were welded at a constant speed of 10 cm/min at 160 A and 30 cm/min at 140 A. A bead-on-plate weld was performed. The weld had a length of 50 mm. After the LIBS laser was started, the argon shielding gas stream began to flow. Then, the welding plasma ignited and the table started, so the specimen was moved until the 50 mm was reached. The welding torch was turned off and the argon shielding gas flow remained for 3 s after the end of the welding process. The LIBS laser ended after the specimen reached 150 °C. The surface temperature in the molten pool was measured using a pyrometer from Advanced Energy. Furthermore, a thermocouple was placed in the heat-affected zone. The laser was focused on the specimen 10 mm behind the point at which the tungsten electrode was directed (see Fig. 3). This minimized influences from the welding plasma and the argon shielding gas. The *in situ* LIBS measurements were performed directly behind the welding torch. Fig. 3 shows the start and end points of the laser and the welding torch. Furthermore, the LIBS measurements on the weld seam are visible.

3. Results and discussion

3.1. Creation of calibration curves for quantitative LIBS measurement

Typically, the overall goal of most chemical measurement methods is to provide a quantitative measurement with the highest possible precision. A considerable amount of literature has been published on calibration methods and their processes [36,37]. Experimental calibrations are carried out by measuring a set of calibration samples containing the analyte (or analytes) under investigation in sensibly graded amounts. As calibration samples, the analyst uses materials whose contents are known with the highest possible reliability, i.e., which are both correct and precise. The contents of these calibration samples can be regarded as error-free compared to the measurement results. The important thing in a quantitative measurement with LIBS is to ensure the same measurement conditions during calibration and measurement of the unknown sample. The advantage of LIBS is that the samples require little preparation in advance to perform measurements. To perform a quantitative measurement using the LIBS method, calibration curves must be established. In general, univariate and multivariate calibrations are distinguished. The biggest difference between the two methods is the effort in

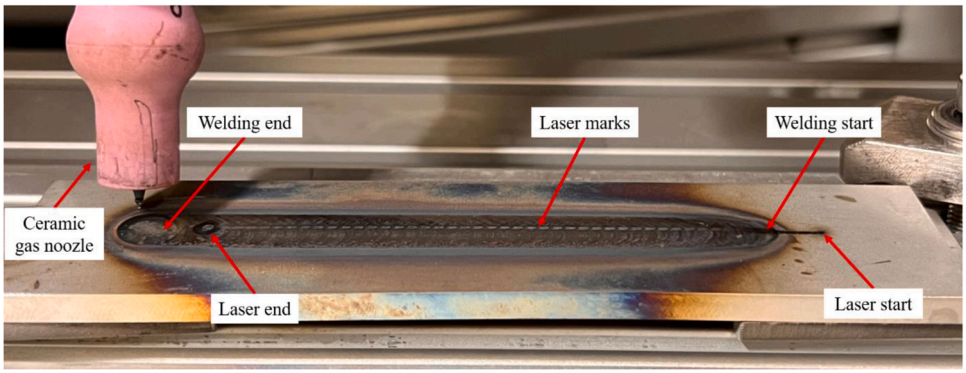

Fig. 3. Weld seam with LIBS Laser marks. Start and end point of the welding process and the laser are marked.

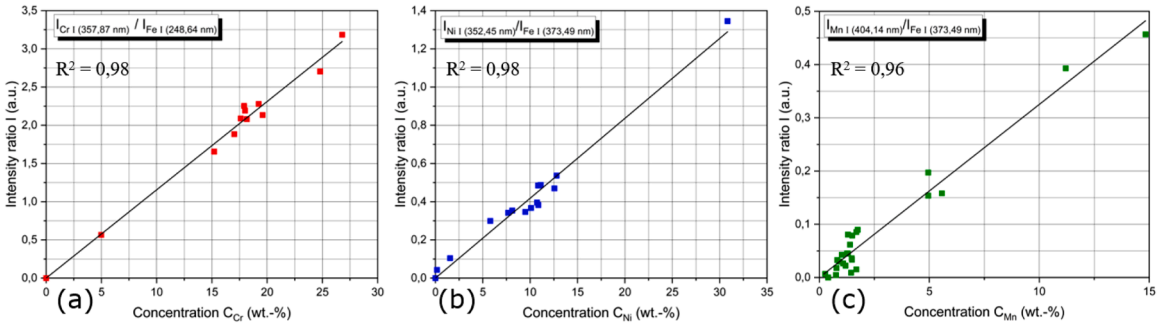

Fig. 4. Calibration curves for the main alloying elements (a) chromium; $R^2 = 0.98$, (b) nickel; $R^2 = 0.98$ and (c) manganese; $R^2 = 0.96$.

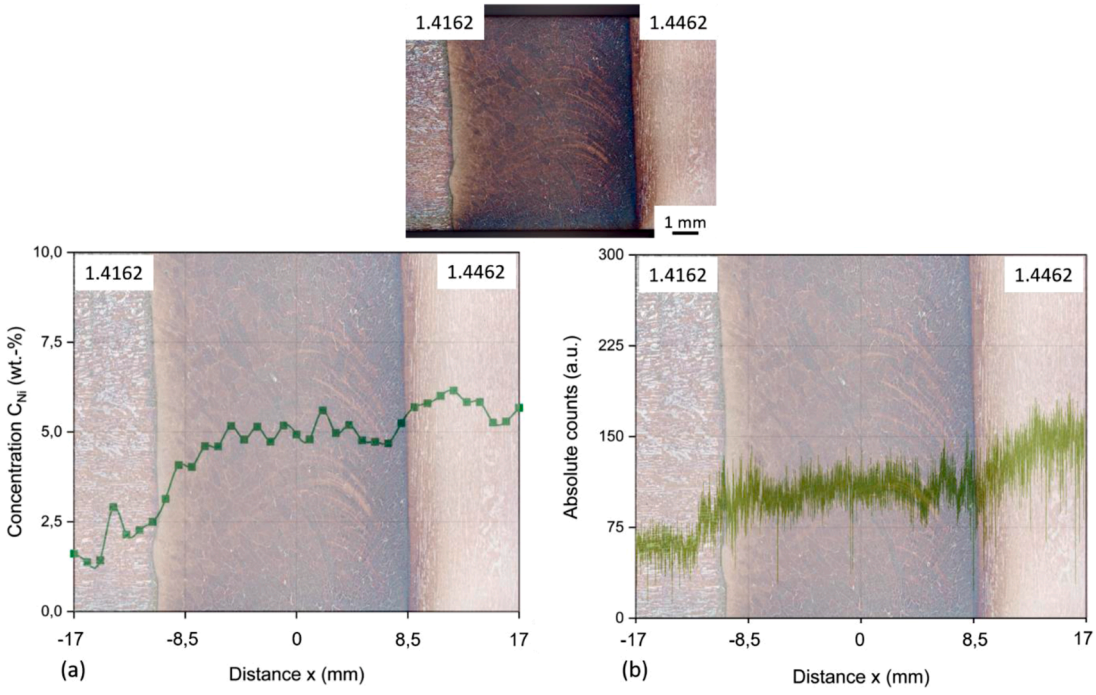

Fig. 5. Butt weld of duplex steals EN grade 1.4162 and 1.4462. (a) LIBS measurement across the weld seam and quantitative analysis of the Ni concentration. (b) EDX measurement across the weld seam. The increase in nickel concentration is clearly visible in both measurement methods.

calculating the models. Univariate models are mostly linear regression models that can be created with manageable effort. Multivariate models, such as Partial Least Squares (PLS) analysis, require a large amount of time to create and validate the models [37].

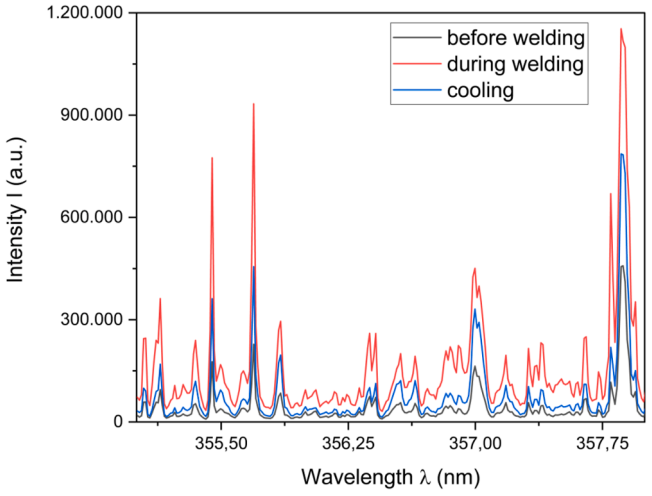

Fig. 6. LIBS Intensities for different stages during a welding process. Welding properties: 140 A, 30 cm/min, gas flow rate 10 l/min.

A univariate method was selected for the initial generation of calibration curves. For this purpose, 30 certified stainless steel reference materials were obtained from various steel manufacturers. In order to produce a satisfactory calibration, some properties of the LIBS lines must be taken into account. They should not be self-absorbed, should not be influenced by other emitting element lines and the background of the spectrum should be subtracted [23,38,39]. Table 3 shows selected wavelengths for the main alloying elements Cr, Ni, Mn and the matrix element Fe. The resulting calibration curves are shown in Fig. 4. The calibration is satisfactory due to the high coefficients of determination (Chromium: $R^2 = 0.98$, Nickel: $R^2 = 0.98$; Manganese: $R^2 = 0.96$) and can be used for a measurement of samples with unknown chemical compositions.

3.2. *Verification of the LIBS measurement method with EDX analysis*

To validate the *in situ* measurement method LIBS, analyses of a butt weld of a lean duplex EN grade 1.4162 and a standard duplex EN grade 1.4462 were carried out. The welding current was 120 A and the

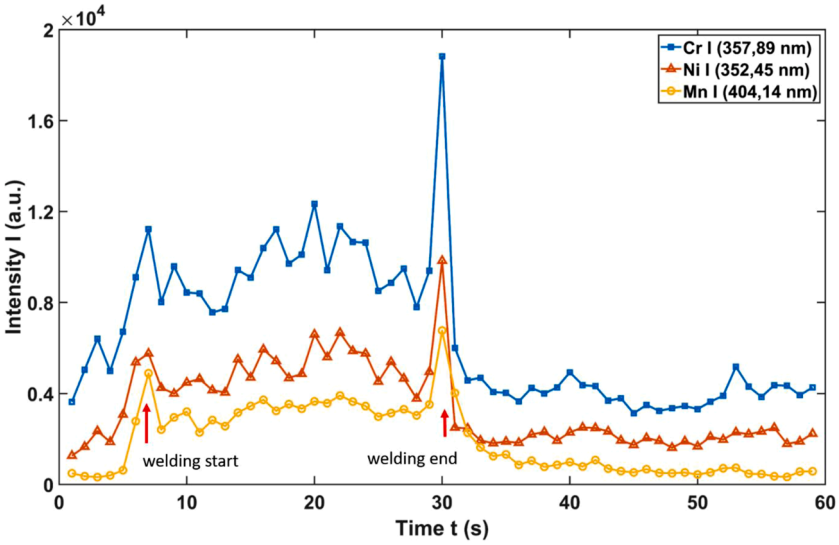

Fig. 7. LIBS intensities of the main alloying elements during the TIG welding process. Weld parameters: 160 A, 10 cm/min, gas flow rate 10 l/min; welding start at t = 7 s, welding end at t = 31 s.

welding speed was 10 cm/min. No filler metal was used.

The Ni concentration over the weld seam of the butt weld was quantitatively analyzed using LIBS and compared with a conventional measurement method EDX in a scanning electron microscope. The results are shown in Fig. 5. The curves of the two measuring methods show a high agreement. In particular, the increase in nickel concentration compared to the standard duplex 1.4462 is clearly visible in both measuring methods. With the aid of the previously generated calibration curves, a quantitative statement of the nickel concentration on the weld seam can be made. The nickel concentrations in the base metal of the two DSS are in high agreement with the results of the chemical analysis (1.4162 C_{Ni}: 1.54 wt.-%; 1.4462 C_{Ni}: 5.79 wt.-%). Based on this satisfactory validation of the LIBS measurement method, *in situ* welding tests can now be carried out.

3.3. *In situ monitoring of element concentrations during TIG welding*

Fig. 6 shows sections of LIBS spectra from different points in time during TIG welding. A DSS EN grade 1.4162 was welded with a welding current of 140 A and a welding speed of 30 cm/min. The intensities before, during and after welding can be seen. It is noticeable that the intensities increase sharply during welding. The LIBS intensities strongly depend on ambient conditions. Initially, the LIBS plasma is ignited in an atmospheric environment. Just before the welding process, the shielding gas Ar is turned on and creates an argon atmosphere on the surface of the specimen. In different gases, the LIBS plasma expands differently [40–42]. Due to the additional electromagnetic radiation from the welding plasma during the welding process, radiation from both the welding plasma and the LIBS plasma is collected in the spectrometer. This leads to an increase in the intensities. In the cooling process, the intensities are still above the intensities before welding. This phenomenon was already observed by Taparli et al. [24]. Since the temperature of the specimen during cooling is higher than before welding, the intensities are higher [27,28]. These three reasons (environment, welding plasma, temperature dependence of the LIBS intensities) lead to the increase of the LIBS intensities during the welding process and during cooling, which can be seen in Fig. 6.

Looking at the intensities of the main alloying elements Cr, Ni and Mn over the entire welding process (Fig. 7), the phenomenon of increasing LIBS intensities can be examined in more detail. Here, a DSS EN grade 1.4462 was used with a welding current of 160 A and a welding speed of 10 cm/min. Similar curves can be seen for all elements.

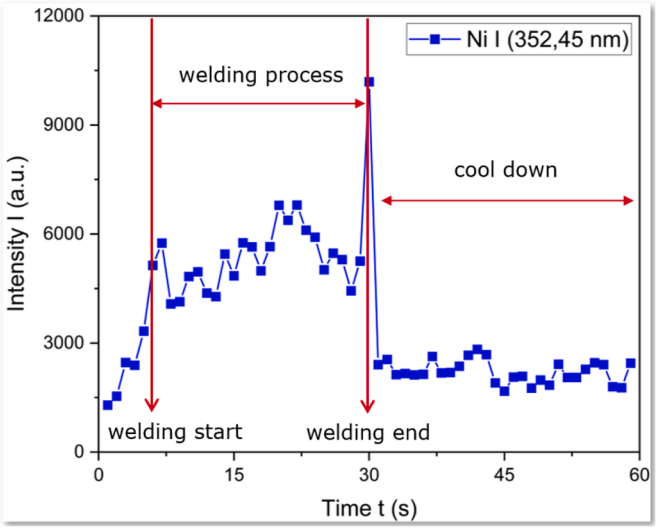

Fig. 8. Nickel intensities as a function of time during TIG welding process; Weld parameters: 160 A and 10 cm/min, gas flow rate 10 l/min.

The LIBS intensities are directly related to the concentration in the material [43]. Therefore, the Cr intensities (C_{Cr} = 22.65 wt.-%) are significantly higher than the Ni (C_{Ni} = 5.79 wt.-%) and Mn intensities (C_{Mn} = 1.68 wt.-%).

From the Ni concentration in Fig. 8, the different stages of the *in situ* measurement of the welding process can be elicited. At t = 7 s the welding process starts. Due to the formation and spreading of the welding plasma, a strong increase of the intensities can be seen. During the welding process (t = 8–30 s), the intensities remain almost constant, but increased. At the end of the welding process (t = 31 s), the same phenomenon as at the start of the welding process (t = 7 s) can be seen. After the end of the welding process (t = 31 s), the cooling process begins (t = 32–60 s). The intensities decrease steadily. This is because the intensities are dependent on the surface temperature [27,28].

With the aid of the calibration curves obtained, the concentrations during the welding process can now be determined. First, the nickel intensities must be normalized to the iron intensities. This is a common procedure to minimize stochastic effects when generating laser plasmas on the surface [36]. The laser light from each laser pulse, while

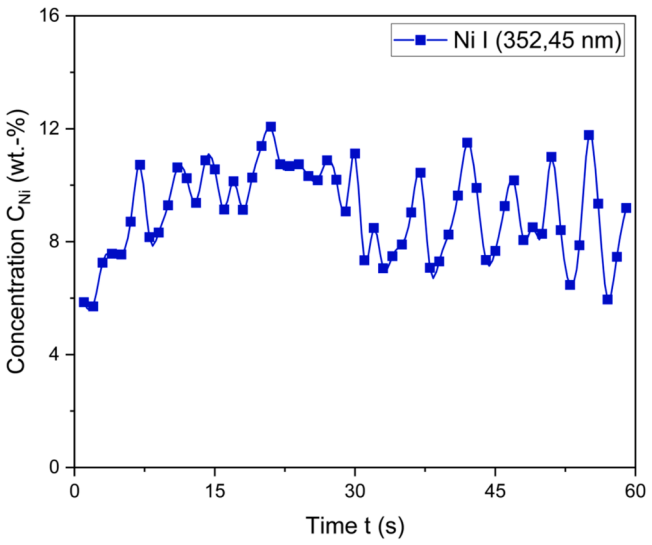

Fig. 9. Nickel concentration CNi during TIG welding of EN grade 1.4462. The line is a guide-to-the-eye. Weld parameters: 160 A, 10 cm/min, gas flow rate 10 l/min.

Table 2
Main alloying elements of EN grade 1.4462 and 1.4162; measured with spark emission spectroscopy.

Grade	Main alloying elements (wt.%)						
	C	Cr	Ni	Mn	Si	Mo	Fe
1.4462	0.020	22.650	5.790	1.680	0.320	2.970	bal.
1.4162	0.018	21.940	1.540	4.950	0.600	0.310	bal.

irradiance remains constant, is reflected and absorbed differently by the sample. This leads to a variation in the LIBS intensity. To increase the repeatability of the LIBS measurements, the trace element (Ni) is normalized to the matrix element (Fe). Subsequently, the LIBS intensities can be converted into concentrations during the welding process using the previously determined calibration curves. In Fig. 9, the nickel concentration during TIG welding of an EN grade 1.4462 is shown. The welding current was 160 A and the welding speed was 10 cm/min. Since the first measurements were performed on the base metal, the nickel concentration before the welding process ($t = 1$ s) is $C_{Ni} = 5.80$ wt.% (cf. OES measurement $C_{Ni} = 5.79\%$). During the welding process ($t = 8$–30 s), the Ni concentration increases and remains relatively constant at a value of $C_{Ni} = 10$ wt.%. After the end of the welding process ($t > 30$ s), the Ni concentration fluctuates strongly, but is on average about $C_{Ni} = 8$ wt.%. The concentration in the weld metal is therefore higher than in the base metal. This can be explained by the evaporation of the alloying elements during welding. During welding, metal vapor can be released from the surface of the weld pool. The evaporation of alloying elements from the weld pool is a complex process and can be found in the literature [44,45]. Presumably, C_{Ni} is higher due to evaporation during welding. After welding, C_{Ni} is slightly lower however higher than in the base metal because of a nickel layer on the surface of the weld metal. Taparli et al. [26] already found that alloying elements accumulate on the weld after TIG welding of stainless steels. This could now be determined with the aid of LIBS during TIG welding.

This loss of material inevitably leads to a change in the chemical composition of the weld metal. This loss of material may cause a change in the microstructure, as well as a degradation of the mechanical properties of the weld metal. To increase the prediction accuracy of the ferrite content and optimize the WRC-1992 diagram, the LIBS experiments need to be further optimized. Especially the variation of the concentrations after the welding process must be minimized. The so-called matrix effect can be an influencing factor on the quality of the LIBS measurement. Depending on the structural and chemical composition of the measured sample, the laser-material interaction is influenced [46,47]. In the future, calibration will be performed using multivariate models. This should minimize interfering factors and increase the quality of the LIBS measurements. PLS models are to be created for future investigations. For the used spectrometer Aryelle 400 there are already works, in which PLS models for calibration were created [48] (Table 2).

Table 3
Selected wavelengths for calibration for the main alloying elements Cr, Ni, Mn and the matrix element Fe.

Element	Wavelength
Cr I	357.87 nm
Ni I	352.45 nm
Mn I	404.14 nm
Fe I	373.49 nm

4. Conclusions

In situ investigations of TIG welding tests combined with LIBS measurements on DSS have been successfully carried out. LIBS is suitable for visualizing the chemical concentration during welding. The main findings resulting from the experiments are.:

- LIBS spectral intensities increase during TIG welding of DSS. The LIBS intensities are temperature dependent and increase with increasing specimen temperature.
- Univariate calibration curves could be established using certified reference materials and provided satisfactory calibration for the main alloying elements Cr, Ni and Mn.
- The course of the nickel concentration could be shown *in situ* during TIG welding of DSS. The nickel concentration increases virtually during the welding process. The nickel concentration is higher than the nickel concentration in the base metal after the welding process.

For future research, PLS models are to be used for quantitative measurement. This should calculate the concentration more precisely and minimize the influence of various interfering factors. Furthermore, electron temperatures during the TIG welding process will be calculated using LIBS intensities and correlated with surface temperatures. To optimize the WRC1992 diagram, further research work has to be carried out and several tests with various welding parameters have to be performed.

Declaration of Competing Interest

The authors declare that they have no known competing financial interests or personal relationships that could have appeared to influence the work reported in this paper.

Acknowledgments

funded by the Deutsche Forschungsgemeinschaft (DFG, German Research Foundation) – 442001176.

References

[1] I. Alvarez-Armas, Duplex stainless steels: brief history and some recent alloys, Recent Pat. Mech. Eng. 1 (1) (2008) 51–57 [Online]. Available, https://www.ingentaconnect.com/content/ben/meng/2008/00000001/00000001/art00006.
[2] K.H. Lo, C.H. Shek, J. Lai, Recent developments in stainless steels, Mater. Sci. Eng. R Rep. 65 (4–6) (2009) 39–104.

[3] E.M. Westin, C.O.A. Olsson, S. Hertzman, Weld oxide formation on lean duplex stainless steel, Corros. Sci. 50 (9) (2008) 2620–2634, https://doi.org/10.1016/j.corsci.2008.06.024, 2008/09/01/.

[4] J. Yang, Q. Wang, Z. Wei, K. Guan, Weld failure analysis of 2205 duplex stainless steel nozzle, Case Stud. Eng. Fail. Anal. 2 (2) (2014) 69–75, https://doi.org/10.1016/j.csefa.2014.05.001, 2014/10/01/.

[5] G. Martin, et al., A macro-and micromechanics investigation of hot cracking in duplex steels, Acta Mater. 60 (11) (2012) 4646–4660.

[6] S.S. Babu, J.M. Vitek, Y.S. Iskander, S.A. David, New model for prediction of ferrite number of stainless steel welds (in English), Sci. Technol. Weld. Join. 2 (6) (1997) 279–285, https://doi.org/10.1179/stw.1997.2.6.279.

[7] A. Moteshakker, I. Danaee, Microstructure and corrosion resistance of dissimilar weld-joints between duplex stainless steel 2205 and austenitic stainless steel 316L, J. Mater. Sci. Technol. 32 (3) (2016) 282–290, https://doi.org/10.1016/j.jmst.2015.11.021, 2016/03/01/.

[8] M.A. Makhdoom, A. Ahmad, M. Kamran, K. Abid, W. Haider, Microstructural and electrochemical behavior of 2205 duplex stainless steel weldments, Surf. Interfaces 9 (2017) 189–195, https://doi.org/10.1016/j.surfin.2017.09.007, 2017/12/01/.

[9] A.L. Schaeffler, Selection of austenitic electrodes for welding dissimilar metals, Weld. J. 26 (1947) 601–620.

[10] W.T. Delong, "Constitution diagram for stainless-steel weld metal .1. Delong diagram," (in English), Met Prog, vol. 106, no. 1, pp. 226, 1974. [Online]. Available: <Go to ISI>://WOS:A1974T371300066.

[11] D.J. Kotecki, T.A. Siewert, Wrc-1992 constitution diagram for stainless-steel weld metals - a modification of the Wrc-1988 diagram (in English), Weld. J. 71 (5) (1992) S171–S178. May[Online]. Available: <Go to ISI>://WOS:A1992HR96600017.

[12] M. Vasudevan, A. Bhaduri, B. Raj, Prediction of ferrite number in stainless steel welds using Bayesian neural network model, Weld. World 51 (7) (2007) 15–28.

[13] B. Arivazhagan, M. Vasudevan, Studies on A-TIG welding of 2.25Cr-1Mo (P22) steel (in English), J. Manuf. Process. 18 (2015) 55–59, https://doi.org/10.1016/j.jmapro.2014.12.003. Apr.

[14] Schweißen– Bestimmung der Ferrit-Nummer (FN) in austenitischem und ferritisch-austenitischem (Duplex-)Schweißgut von Cr-Ni-Stählen (ISO/DIS8249:2017); Deutsche und Englische Fassung prEN ISO 8249:2017, D. E. I. 8249, 2017.

[15] S. Wessman, Evaluation of the WRC 1992 diagram using computational thermodynamics, Weld. World 57 (3) (2013) 305–313, https://doi.org/10.1007/s40194-013-0025-7, 2013/05/01.

[16] D.J. Kotecki, V.B. Rajan, Submerged arc fillet welds between mild steel and stainless steel (in English), Weld. J. 76 (2) (1997) S57–S66. Feb[Online]. Available: ≤Go to ISI≥://WOS:A1997WF78500022.

[17] M.C. Balmforth, J.C. Lippold, A new ferritic-martensitic stainless steel constitution diagram, Weld. J. 79 (12) (2000) 339–345.

[18] F. Giudice, A. Sili, Weld metal microstructure prediction in laser beam welding of austenitic stainless steel, Appl. Sci. 11 (4) (2021) 1463.

[19] S.I. Shah, H.R. Thakkar, K. Patel, G.D. Acharya, Investigation of microstructure and mechanical properties of DSS 2205 weld thick section for pressure vessel application, Trans. Indian Inst. Met. (2021), https://doi.org/10.1007/s12666-021-02284-9, 2021/06/07.

[20] S. Zhang, Q. Wang, R. Yang, C. Dong, Composition equivalents of stainless steels understood via gamma stabilizing efficiency, Sci. Rep. 11 (1) (2021) 5423, https://doi.org/10.1038/s41598-021-84917-z, 2021/03/08.

[21] M.A.V. Bermejo, A mathematical model to predict δ-ferrite content in austenitic stainless steel weld metals, Weld. World 56 (9) (2012) 48–68.

[22] M.A. Valiente Bermejo, D. Eyzop, K. Hurtig, L. Karlsson, Welding of large thickness super duplex stainless steel: microstructure and properties, Metals 11 (8) (2021) 1184.

[23] R. Noll, Laser-Induced Breakdown Spectroscopy Fundamentals and Applications, Springer, Berlin, 2012 (in eng).

[24] U.A. Taparli, L. Jacobsen, A. Griesche, K. Michalik, D. Mory, T. Kannengiesser, *In situ* laser-induced breakdown spectroscopy measurements of chemical compositions in stainless steels during tungsten inert gas welding, Spectrochim. Acta Part B At. Spectrosc. 139 (2018) 50–56, https://doi.org/10.1016/j.sab.2017.11.012, 2018/01/01/doi:.

[25] U.A. Taparli, T. Kannengiesser, K. Cieslik, D. Mory, A. Griesche, *In situ* chemical composition analysis of a tungsten-inert-gas austenitic stainless steel weld measured by laser-induced breakdown spectroscopy, Spectrochim. Acta Part B At. Spectrosc. (2020), 105826, https://doi.org/10.1016/j.sab.2020.105826, 2020/03/12/doi:.

[26] U.A. Taparli, T. Kannengiesser, A. Griesche, Tungsten inert gas bead-on-plate weld chemical composition analysis by laser-induced breakdown spectroscopy, in: Proceedings of the IOP Conference Series: materials Science and Engineering 882, 2020, 012023, https://doi.org/10.1088/1757-899x/882/1/012023, 2020/08/29.

[27] S.M.R. Darbani, M. Ghezelbash, A.E. Majd, M. Soltanolkotabi, H. Saghafifar, Temperature effect on the optical emission intensity in laser induced breakdown spectroscopy of super alloys (in English), J. Eur. Opt. Soc. Rapid 9 (2014) 14058: 1–14058:8 [Online]. Available: ≤Go to ISI≥://WOS:000346896900001.

[28] S.H. Tavassoli, A. Gragossian, Effect of sample temperature on laser-induced breakdown spectroscopy, Opt. Laser Technol. 41 (4) (2009) 481–485, https://doi.org/10.1016/j.optlastec.2008.07.010, 2009/06/01/.

[29] R. Sanginés, H. Sobral, E. Alvarez-Zauco, The effect of sample temperature on the emission line intensification mechanisms in orthogonal double-pulse laser Induced breakdown spectroscopy, Spectrochim. Acta Part B At. Spectrosc. 68 (2012) 40–45, https://doi.org/10.1016/j.sab.2012.01.011, 2//.

[30] J. Mirapeix, P.B. Garcia-Allende, O.M. Conde, J.M. Lopez-Higuera, A. Cobo, Welding diagnostics by means of particle swarm optimization and feature selection, J. Sens. 2012 (2012) 11, https://doi.org/10.1155/2012/318038. Art no. 318038.

[31] P.B. Garcia-Allende, J. Mirapeix, O.M. Conde, A. Cobo, J.M. Lopez- Higuera, Arc-welding spectroscopic monitoring based on feature selection and neural networks, Sensors 8 (10) (2008) 6496–6506, https://doi.org/10.3390/s8106496.

[32] V.N. Lednev, et al., Online and *in situ* laser-induced breakdown spectroscopy for laser welding monitoring, Spectrochim. Acta Part B At.c Spectrosc. (2020), 106032, https://doi.org/10.1016/j.sab.2020.106032, 2020/11/29/doi:.

[33] V.N. Lednev, et al., *In situ* laser-induced breakdown spectroscopy measurements during laser welding of superalloy, App.l Opt. 60 (5) (2021) 1144–1149, https://doi.org/10.1364/AO.411359, 2021/02/10.

[34] S. Kou, Welding Metallurgy, 2nd ed., Wiley-Interscience, Hoboken, NJ, 2003 (in eng).

[35] M. Mueller, I.B. Gornushkin, S. Florek, D. Mory, U. Panne, Approach to detection in laser-induced breakdown spectroscopy, Anal. Chem. 79 (12) (2007) 4419–4426, https://doi.org/10.1021/ac0621470, 2007/06/01doi:.

[36] D.A. Cremers, L.J. Radziemski, Handbook of Laser-Induced Breakdown Spectroscopy, 2nd ed., Wiley, Chichester, 2006 (in eng).

[37] M.A. Sharaf, D.L. Illman, B.R. Kowalski, Chemometrics, John Wiley & Sons, 1986.

[38] L. Paksy, B. Német, A. Lengyel, L. Kozma, J. Czekkel, Production control of metal alloys by laser spectroscopy of the molten metals. Part I. Preliminary investigations, Spectrochim. Acta Part B At. Spectrosc. 51 (2) (1996) 279–290, https://doi.org/10.1016/0584-8547(95)01340-7, 1996/01/30/doi:.

[39] J. Vrenegor, R. Noll, V. Sturm, Investigation of matrix effects in laser-induced breakdown spectroscopy plasmas of high-alloy steel for matrix and minor elements, Spectrochim. Acta Part B At. Spectrosc. 60 (7–8) (2005) 1083–1091.

[40] A.C.F. Anabiarte, J.M. Lopez-Higuera, Laser-induced breakdown spectroscopy: fundamentals, applications, and challenges, ISRN Spectrosc. 2012 (2012), https://doi.org/10.5402/2012/285240. Review Article.

[41] A.J. Effenberger, J.R. Scott, Effect of atmospheric conditions on LIBS spectra (in English), Sensors 10 (5) (2010) 4907–4925, https://doi.org/10.3390/s100504907. May.

[42] A. Löbe, J. Vrenegor, R. Fleige, V. Sturm, R. Noll, Laser-induced ablation of a steel sample in different ambient gases by use of collinear multiple laser pulses, Anal. Bioanal. Chem. 385 (2) (2006) 326–332, https://doi.org/10.1007/s00216-006-0359-8, journal article.

[43] D.W. Hahn, N. Omenetto, Laser-Induced Breakdown Spectroscopy (LIBS), part II: review of instrumental and methodological approaches to material analysis and applications to different fields, Appl. Spectrosc. 66 (4) (2012) 347–419, https://doi.org/10.1366/11-06574.

[44] H. Park, M. Trautmann, K. Tanaka, M. Tanaka, A.B. Murphy, A computational model of gas tungsten arc welding of stainless steel: the importance of considering the different metal vapours simultaneously, J. Phys. D Appl. Phys. 51 (39) (2018), 395202, https://doi.org/10.1088/1361-6463/aad74c, 2018/08/22.

[45] M.M. Collur, A. Paul, T. Debroy, Mechanism of alloying element vaporization during laser-welding (in English), Metall. Trans. B 18 (4) (1987) 733–740, https://doi.org/10.1007/Bf02672891. Dec.

[46] C. Aragón, J.A. Aguilera, Characterization of laser induced plasmas by optical emission spectroscopy: a review of experiments and methods, Spectrochim. Acta Part B At. Spectrosc. 63 (9) (2008) 893–916, https://doi.org/10.1016/j.sab.2008.05.010, 9//.

[47] J.A. Aguilera, C. Aragón, Characterization of a laser-induced plasma by spatially resolved spectroscopy of neutral atom and ion emissions.: comparison of local and spatially integrated measurements, Spectrochim. Acta Part B At. Spectrosc. 59 (12) (2004) 1861–1876.

[48] S. Merk, C. Scholz, S. Florek, D. Mory, Increased identification rate of scrap metal using laser induced breakdown spectroscopy echelle spectra (in English), Spectrochim. Acta B 112 (2015) 10–15, https://doi.org/10.1016/j.sab.2015.07.009. Oct 1.